DTU Library

A model for the static properties of DH lasers

Buus, Jens

Link back to DTU Orbit

A Model for the Static Properties of DH Lasers

JENS BUUS, MEMBER, IEEE

Abstract—The various subproblems for DH lasers such as field distribution, carrier profile, and temperature distribution are investigated. Solutions to these problems are obtained either analytically or by precise numerical methods.

By combining the subproblems, a detailed model for the static properties is obtained. The model is applicable as well below as above threshold and properties of interest in the application of DH lasers such as threshold current, field distribution at a given current, and light current characteristics can be found.

Nonlinear characteristics are found even for ideal symmetrical lasers. These "kinks" are associated with higher order modes and appear at relatively high values of the optical power.
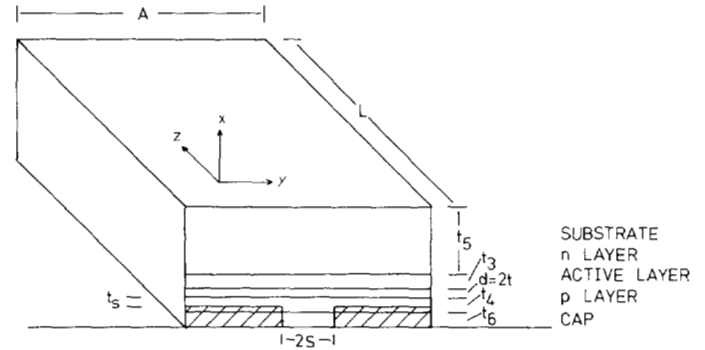

Fig. 1. Structure of DH stripe laser.

I. INTRODUCTION

THE DH lasers under consideration are described by the structure shown in Fig. 1.

The hatched area in Fig. 1 is the proton bombarded zone. In case of oxide insulation the thickness of the spreading layer t_s is equal to t_4 (p layer) plus t_6 (cap).

For a given current I, the problem consists in finding the current density distribution J, the temperature T, the carrier density profile N, the intensity distributions I_p, and amplitudes s_p. The lateral modes are denoted by the mode number p. J, T, N, and I_p are functions of the position y in the junction plane.

We start by treating the various problems independently. The method used for solving the field problem is an extension of the results from [1]-[4]. By coupling the problems a model for the laser is obtained. This model is discussed in connection with [6], [7] and some results are presented.

II. SUBPROBLEMS

A. Formulation of Field Problem

When variations of the field distribution with length (z direction in Fig. 1) are neglected the field problem is two dimensional. The complex permittivity is a function of the x and y positions and is approximately given by

$$\epsilon(x, y) = \begin{cases} \epsilon_1(y) \approx n_1(y)^2 + j\dfrac{n_1(y)g_1(y)}{k} & |x| \leqslant t \\ \epsilon_2(y) \approx n_2(y)^2 + j\dfrac{n_2(y)g_2(y)}{k} & |x| > t. \end{cases} \quad (1)$$

n, g, and k are the refractive index, gain, and free space propagation constant, respectively. Index 1 refers to the active layer

and index 2 refers to the confinement layers. In all practical cases $n \gg |g|/k$ and the approximation leading to (1) consists of neglecting $(g/2k)^2$ compared to the other terms.

The difference between the refractive indexes n_1 and n_2 is due to different aluminum content inside the active layer and in the n and p layers. This difference is several orders of magnitude larger than the y variation of n_1 and n_2.

With ϵ given by (1) we cannot solve the field problem directly by separating the x variation and the y variation. Using the "effective dielectric constant," e.g., [1], however, we obtain the following equation for the y variation of TE modes [2]:

$$\frac{d^2 y}{dy^2} + (\beta_y^2 + (\epsilon_{\text{eff}}(y) - \epsilon_{\text{eff}}(0)) k^2) Y = 0 \quad (2)$$

where $\beta_y^2 \approx \Lambda_p, p = 0, 1, \cdots$ are eigenvalues and

$$\epsilon_{\text{eff}}(y) = b\epsilon_1(y) + (1 - b)\epsilon_2(y). \quad (3)$$

b is the normalized propagation constant.

We only consider the fundamental mode in the x direction and it can be shown that b can be interpreted as a field filling factor [2].

According to Schlosser [3] the difference between the imaginary parts of ϵ_1 and ϵ_2 gives rise to a small imaginary part of b but leaves the real part unchanged. Hence, $b = b_0 + jb_i$ where b_0 is determined from n_1, n_2 and the thickness of the active layer.

Since $n_1 \gg |g_1|/k$, $n_2 \gg |g_2|/k$, and $(n_1 - n_2) \gg |g_1 - g_2|/k$ we get

$$\epsilon_{\text{eff}}(y) = b_0 \left(n_1(y)^2 + j\frac{n_1(y)g_1(y)}{k} \right)$$

$$+ (1 - b_0) \left(n_2(y)^2 + j\frac{n_2(y)g_2(y)}{k} \right)$$

$$+ jb_i(y) (n_1(y)^2 - n_2(y)^2) \quad (4)$$

where [3]

$$b_i(y) = \frac{1}{2k} \frac{g_1(y) - g_2(y)}{n_1(y) - n_2(y)} \frac{(1 - b_0) v_0 \sqrt{b_0}}{1 + v_0 \sqrt{b_0}}. \tag{5}$$

v_0 is the normalized frequency which is considered constant because of the small variations of n_1 and n_2 with y. Hence,

$$v_0 = kt \sqrt{n_1(0)^2 - n_2(0)^2}. \tag{6}$$

The intensity filling factor Γ, which is the fraction of the intensity propagation in the active layer, can be written [2], [3]

$$\Gamma = \frac{\displaystyle\int_{-t}^{t} I(x)\, dx}{\displaystyle\int_{-\infty}^{\infty} I(x)\, dx} = b_0 + \frac{(1 - b_0) v_0 \sqrt{b_0}}{1 + v_0 \sqrt{b_0}} \tag{7}$$

where $I(x)$ is the intensity distribution in the x direction. When (5) and (7) are introduced in (4) we get

$$\epsilon_{\text{eff}}(y) = b_0 n_1(y)^2 + (1 - b_0) n_2(y)^2$$
$$+ j \frac{n_{\text{eff}}(0)}{k} (\Gamma g_1(y) + (1 - \Gamma) g_2(y)) \tag{8a}$$

$$n_{\text{eff}}(0) = \sqrt{b_0 n_1(0)^2 + (1 - b_0) n_2(0)^2}. \tag{8b}$$

This expression shows that ϵ_{eff} can be considered as an average of ϵ_1 and ϵ_2, the real parts being weighted by b_0 but the imaginary parts by Γ. In [4] Γ was used for both the real and the imaginary parts and in [2] b_0 was used in both cases.

The ratio of the variations in the real part of ϵ_{eff} to the imaginary part depends on b_0 and Γ which are both functions of the normalized frequency v_0 [3], and hence depends on the thickness of the active layer (6).

Using the assumptions that $g_2(y)$ is constant, n_1 varies with temperature and electron density, and n_2 varies with temperature only, (8) yields

$$\epsilon_{\text{eff}}(y) - \epsilon_{\text{eff}}(0) = 2 b_0 n_1(0) \frac{\delta n}{\delta N} (N(y) - N(0))$$

$$+ 2 n_{\text{eff}}(0) \frac{\delta n}{\delta T} (T(y) - T(0))$$

$$+ j \Gamma n_{\text{eff}}(0) \frac{g_1(y) - g_1(0)}{k}. \tag{9}$$

Threshold currents are almost exponentially depending on the temperature due to the temperature dependence of the gain. We write the gain for the stimulated emission as a function of temperature and electron density:

$$g(y) = a(T) \cdot N(y) - b_1 \tag{10a}$$

$$a(T) = a_1 - a'(T(y) - T') \tag{10b}$$

$$a' = \frac{a_1}{T_0}, \qquad a_1 = a(T') \tag{10c}$$

where a_1, a', and b_1 are constants and T' the heat sink temperature. Equations (10b)-(10c) are obtained by expanding

an exponentially varying gain described by the characteristic temperature T_0 to the first order. The thermal variation of the gain given by (10) is consistent with the light current characteristics at various temperatures reported in [5].

The net gain in the active layer g_1 is found by subtracting a loss term

$$g_1(y) = g(y) - a_2 N(y) - b_2 \tag{11}$$

where a_2 and b_2 are constants.

With (9)-(11) the field equation (2) is specified when N and T are known functions of y. It is assumed that the temperature is independent of x within the region of interest.

B. Solution of the Field Problem

The method used for solution of (2) is described in detail in [2] and only the important points will be stated here. The method is a matrix method where the coefficients for an expansion of the solution in Hermite-Gauss functions are found from the eigenvectors and the eigenvalues Λ_p are the eigenvalues of the matrix.

By the following expansion of the permittivity,

$$\epsilon_{\text{eff}}(y) - \epsilon_{\text{eff}}(0) = (\epsilon_{\text{eff}}(y) - \epsilon_{\text{eff}}(\infty)) - (\epsilon_{\text{eff}}(0) - \epsilon_{\text{eff}}(\infty))$$

$$= \sum_n \alpha_n H_n \left(\frac{y}{S'}\right) \exp\left(-\left(\frac{y}{S'}\right)^2\right) - \Delta\epsilon_{\text{eff}}, \tag{12}$$

all matrix elements are found analytically. H_n is the Hermite polynomial of order n and S' a scaling length. This expansion is able to give a very precise fit to the calculated profile.

The complex expansion coefficients are found using the orthogonality of Hermite-Gauss functions

$$\alpha_n = \frac{1}{\sqrt{\pi} \, 2^n n! S'} \int_{-\infty}^{\infty} H_n \left(\frac{y}{S'}\right) (\epsilon_{\text{eff}}(y) - \epsilon_{\text{eff}}(\infty))\, dy. \tag{13}$$

The expansion is possible if

$$(\epsilon_{\text{eff}}(y) - \epsilon_{\text{eff}}(\infty)) \exp\left(+\frac{1}{2}\left(\frac{y}{S'}\right)^2\right) \longrightarrow 0$$

$$\text{for } y \longrightarrow \infty \tag{14}$$

since this function can then be expanded in Hermite-Gauss functions. The matrix elements can be expressed by α_n and the gamma function [2]. With this solution also, mode spacings and far fields are easily found [2].

For the solution of the field problem, $\epsilon(y)$ is often approximated by a parabolic variation, e.g., [5], [6]. This gives directly an analytical solution but it is not possible to obtain a detailed description of ϵ.

In [7] a power series $\epsilon(0) - a^2 y^2 +$ higher order terms is used; the first two terms give a Hermite-Gauss solution and the higher order terms give perturbations. This theory will be discussed in Section V.

Also, some special profiles where (2) can be solved analytically have been investigated, e.g., [8]. These profiles, however, are probably of limited interest for detailed calculations.

C. Electron Density

The electron density N is found from the diffusion equation

$$D \frac{d^2 N}{dy^2} = -\frac{J(y)}{ed} + \frac{N}{\tau_s} + \Gamma g(y) \sum_p s_p I_p(y) \tag{15}$$

where s_p is the amplitude and $I_p(y)$ is the normalized intensity distribution for mode p given by

$$I_p(y) = \frac{|Y_p(y)|^2}{\int_{-\infty}^{\infty} |Y_p(y)|^2 \, dy}. \tag{16}$$

$Y_p(y)$ is the solution of (2) for mode p. If the lifetime τ_s is independent of N (but not necessarily of y), (15) can be written as a linear equation using (10) to give

$$\frac{d^2 N}{dy^2} = N \cdot A'(y) - B'(y)$$

$$A'(y) = \frac{1}{D\tau_s} + \frac{\Gamma}{D}(a_1 - d'(T(y) - 300K)) \sum_p s_p I_p(y)$$

$$B'(y) = \frac{J(y)}{edD} + \frac{b_1 \Gamma}{D} \sum_p s_p I_p(y). \tag{17}$$

A numerical method for solution of this equation is presented in the Appendix.

The current density $J(y)$ is calculated according to [9]

$$J(y) = \begin{cases} J_1 & |y| \leqslant S \\ J_1 \dfrac{1}{\left(1 + \dfrac{y-S}{l_0}\right)^2} & |y| > S. \end{cases} \tag{18}$$

J_1 and l_0 are found from the total current I

$$J_1 = \frac{I_a^2 + I(S/L) - I_a \sqrt{I_a^2 + 2I(S/L)}}{2S^2}$$

$$l_0 = \frac{I_a}{\sqrt{J_1}}. \tag{19}$$

The constant I_a depends on the thickness t_s, the resistivity R_s of the spreading layer, and the exponent nkT/e, $n \approx 2$, from the I-V characteristic. Thus,

$$I_a = \sqrt{2 \frac{nkT}{e} \frac{t_s}{R_s}}. \tag{20}$$

D. Temperature

The temperature variation is found by solving the heat flow equation. In [10] a series expansion for $T(y)$ is given. This result contains the Fourier coefficients for the heat source distribution

$$a_n = \frac{2}{n\pi} \sin(b_n S), \, b_n = \frac{2n\pi}{A}, \qquad n = 1, 2, \cdots \tag{21}$$

when a box shaped distribution is assumed. The local thermal resistance becomes

$$R(y) = \frac{2S}{A}\left(\frac{t}{\sigma_{\text{act}}} + \frac{t_4}{\sigma_p} + \frac{t_6}{\sigma_{\text{cap}}}\right) + \sum_n \frac{a_n \cos(b_n y)}{b_n \sigma_{\text{act}}(r_{1,n} + r_{2,n})} \tag{22}$$

where σ is the heat conductivity in the layers, and $r_{1,n}$ and $r_{2,n}$ are found from the boundary conditions [10]. The temperature is found by multiplying (22) by the dissipated power per area $1/2SL$ ($\hbar\omega/eI - 2P_{\text{out}}$) where $\hbar\omega$ is the photon energy and P_{out} is the stimulated power emitted at each mirror. In case of pulsed operation this expression is multiplied by a duty cycle factor. This factor can also be used to scale the influence of thermal effects. In this treatment only a heat source in the active layer is considered.

Other heat source distributions can be taken into account by using other Fourier coefficients in (22), but due to the heat flow the exact distribution is not important.

Taking the distribution as a constant for $|y| \leqslant S$ followed by a tail for $|y| > S$ we have a position dependence of the same type as the current density (18). Since the current density falls off slowly we can assume the carrier density and dissipated power to be proportional to $J(Y)$ for $|y| \gg S$, and a convenient description of the thermal resistance is then obtained by replacing a_n in (22) with the Fourier coefficients for the current density (18) so that

$$a_n' = \frac{J_1}{J_0} \frac{2}{n\pi} \sin(b_n S) + \frac{J_1}{J_0} l_0^2 \frac{4}{A} \left\{ \frac{1}{l_0} \cos(b_n S) \right.$$

$$+ b_n \cos(b_n S)(\cos(b_n l_0) \, si(b_n l_0) - \sin(b_n l_0)$$

$$\cdot C_i(b_n l_0)) + b_n \sin(b_n S)(\cos(b_n l_0) \, C_i(b_n l_0)$$

$$\left. + \sin(b_n l_0) \, si(b_n l_0)) \right\}$$

$$J_0 = \frac{I}{2SL} \tag{23}$$

where we have used integral sine and cosine

$$s_i(x) = -\int_x^{\infty} \frac{\sin t}{t} \, dt = -\frac{\pi}{2} + \int_0^x \frac{\sin t}{t} \, dt = -\frac{\pi}{2} + S_i(x)$$

$$C_i(x) = -\int_x^{\infty} \frac{\cos t}{t} \, dt. \tag{24}$$

E. Lasing Condition

Spontaneous emission into the lasing modes is neglected; hence, modes at or above the threshold must have gain equal to loss. When the normalized intensity distribution for mode p is

$$I_p(x, y) = I(x) I_p(y), \tag{25}$$

the lasing condition becomes

$$\int_{-\infty}^{\infty} \int_{-\infty}^{\infty} g(x, y) I(x) I_p(y) \, dx \, dy = \alpha_{\text{end}} = \frac{1}{L} \ln\left(\frac{1}{R}\right). \tag{26}$$

The gain g is given by

$$g(x, y) = \begin{cases} g_1(y) & |x| \leqslant t \\ g_2(y) = -\alpha_{\text{out}} & |x| > t. \end{cases} \tag{27}$$

Using the filling factor Γ (7) we get from (26) and (27)

$$\overline{g_{1p}} = \frac{\alpha_{end} + (1 - \Gamma)\alpha_{out}}{\Gamma} = g_{th} \qquad (28)$$

where the average net gain in the active region for mode p is

$$\overline{g_{1p}} = \int_{-\infty}^{\infty} g_1(y) I_p(y) \, dy. \qquad (29)$$

The threshold current is defined as the current for which (28) is satisfied for one mode when all amplitude factors s_p are zero.

The lasing condition can be written in terms of propagation constants, noting that the propagation in the z-direction is described by $e^{-j\beta_z z}$. We start from

$$\beta_x(0, 0)^2 + \beta_y^2 + \beta_z^2 = \epsilon_1(0)k^2 \qquad (30)$$

where

$$\beta_x(0, 0)^2 = \frac{v^2}{t^2}(1 - b_0 - jb_i(0))$$

$$v^2 = k^2 t^2 (\epsilon_1(0) - \epsilon_2(0)). \qquad (31)$$

Using (1), (5), (7), (8b), (27), and (31) we get from (30), when Re $\{\beta_y^2\}$ and high order terms are neglected,

$$2 \operatorname{Im}(\beta_z) = g_1(0) - \frac{\operatorname{Im}\{\beta_x(0, 0)^2\}}{n_{eff}(0)k} - \frac{\operatorname{Im}\{\beta_y^2\}}{n_{eff}(0)k} \qquad (32)$$

where

$$\frac{\operatorname{Im}\{\beta_x(0, 0)^2\}}{n_{eff}(0)k} = g_1(0) - g_1(0)\Gamma + \alpha_{out}(1 - \Gamma). \qquad (33)$$

The two last terms in (32) represent diffraction losses. From the lasing condition

$$2 \operatorname{Im}\{\beta_z\} = \alpha_{end} \qquad (34)$$

we finally get for mode p

$$g_1(0) - \frac{1}{\Gamma} \frac{\operatorname{Im}\{\Lambda_p\}}{n_{eff}(0)k} = \frac{\alpha_{end} + (1 - \Gamma)\alpha_{out}}{\Gamma} \qquad (35)$$

where Λ_p is the eigenvalue for (2).

III. COUPLINGS AMONG PROPERTIES

For a given total current I below threshold, we can find the current density [(18)-(20)], the temperature variation, solve the diffusion equation and then the field equation.

Under lasing conditions the unknowns $N(y)$, $I_p(y)$, and s_p must be found from (2), (15) and (28), or (35). These equations are coupled via (9)-(11) and (16). This is shown schematically in Fig. 2.

In the model we have not taken into account that the current density may depend on the electron density and temperature variation.

IV. APPLICATION OF THE MODEL

Below threshold ($\overline{g_{1p}} < g_{th}$ for all p) the amplitude factors s_p are zero so the last term in (15) vanishes, and the electron density can be calculated. From the electron density and
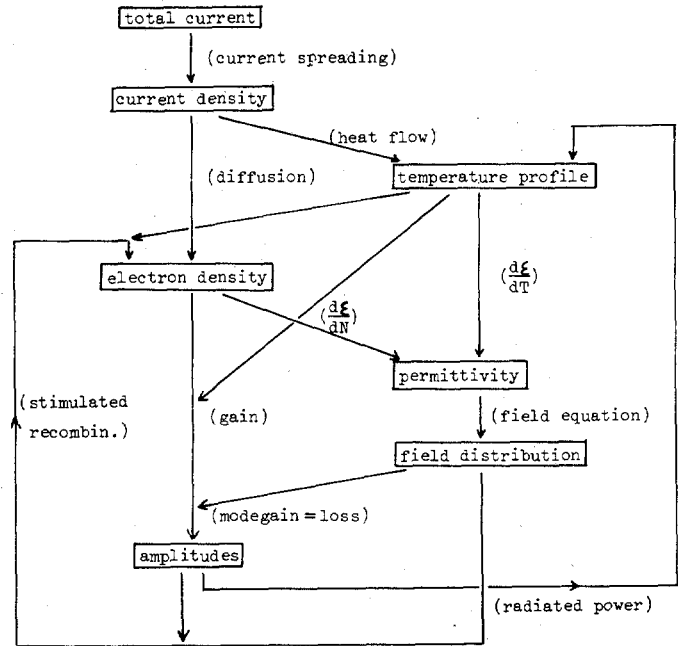

Fig. 2. Graphical representation of the laser model showing properties and couplings taken into account.

temperature the intensity distributions are found. By increasing the current until (28) [or (35)] is satisfied and keeping $s_p = 0$, we find the threshold current. Examples are given in [2].

For currents above threshold simultaneous solutions to (2), (15) and (28), or (35) are found iteratively. We start by setting $s_p = 0$ and then find $N(y)$ and $I_p(y)$. For currents above threshold we use $I_p(y)$ from the previous current value, guess s_p, and calculate $N(y)$. Keeping $I_p(y)$ constant, s_p are varied until $N(y)$ found from (15) satisfies (28) for all modes with $s_p > 0$. Use of (35) during this iteration would require a new calculation of $I_p(y)$ for each new set of s_p values. The resulting values of $N(y)$ are compared with the original and the calculations are repeated until stable solutions for $N(y)$, $I_p(y)$, and s_p are found. The routines for the subproblems have all been tested separately on problems with known solutions.

The amplitudes s_p are related to the stimulated power per mirror by

$$P_{out} = \frac{1}{2} \hbar\omega \ln\left(\frac{1}{R}\right) d \sum_p s_p. \qquad (36)$$

From the calculated amplitudes as a function of the current we get the light current characteristic.

Examples of calculated characteristics are shown in Fig. 3. The various laser parameters used are discussed in [2]. In these examples the power in the fundamental mode saturates at the current value where the next mode starts lasing.

The characteristics have the shape shown in Fig. 4. I_{th} is the threshold current and I_1 is the current where the next mode becomes lasing. Between I_{th} and I_1 the differential efficiency decreases if improved guiding (e.g., due to temperature) decreases the width of the mode.

From various calculations performed we have obtained the following results.
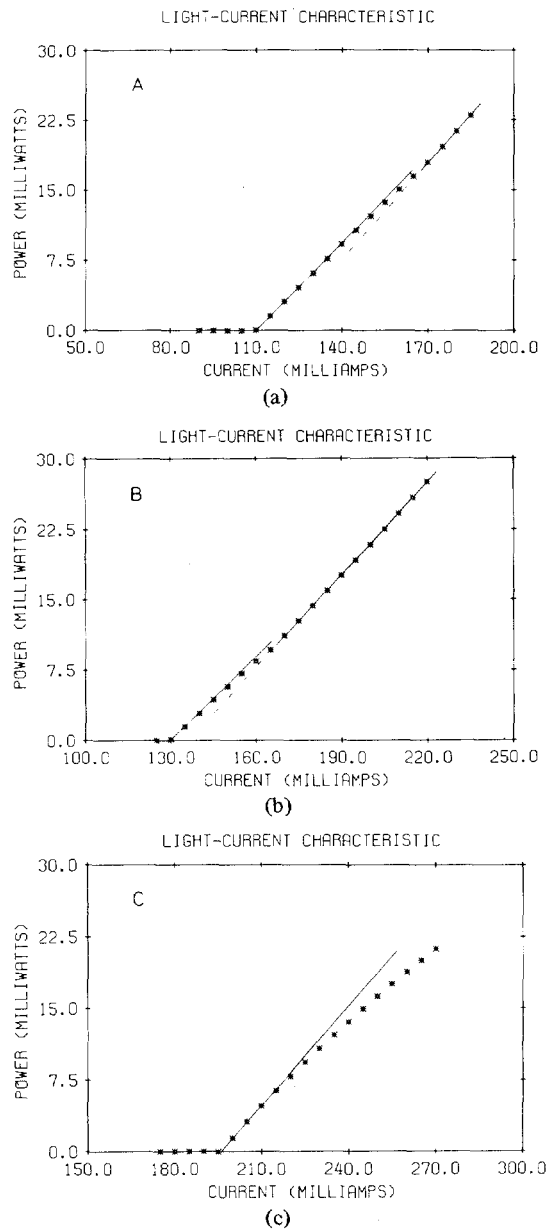
Fig. 3. Light current characteristics: (a) $S = 6$ μm, $d = 0.15$ μm. (b) $S = 8$ μm, $d = 0.15$ μm. (c) $S = 6$ μm, $d = 0.30$ μm.

Fig. 4. Typical light current characteristic (exaggerated).

1) Increasing stripe width decreases P_1.

2) For short diffusion lengths the spatial hole burning is stronger and this decreases P_1.

3) When the length is changed the quantity $(I_1 - I_{th})/I_{th}$ remains almost constant. Since I_{th} decreases faster with decreasing length than the differential efficiency increases, P_1 will decrease.

4) For thick active layers the thermal guiding is relatively weaker and the carriers give a larger negative real part of ϵ_{eff}. This reduced guiding will give a higher P_1.

5) A large number of simulations have been performed using various values of the input parameters. No cases of critical dependence of the result on the input parameters were found.

V. DISCUSSION

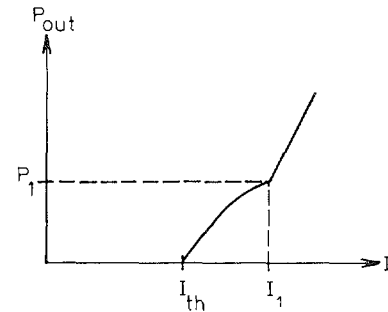In contrast to other theoretical treatments of laser properties the present model offers detailed analytical or numerical solutions to the subproblems. Particularly, the permittivity and field problems are carefully considered. Multimode operation and thermal effects are also included.

In [7] pure gain guiding is assumed. The gain profile is expanded in a power series and a Hermite-Gauss solution is found from the quadratic term. This solution is perturbed by the higher order terms. The present model has been applied to the parameters used in [7]. The calculated characteristic is almost linear, but with the interesting result that $d^2 g_1(y)/dy^2 |_{y=0}$ becomes zero at the power where the kink in [7] is found. This fact indicates that power expansion combined with perturbation theory is not adequate, and that the kink found in [7] can be explained mathematically: a low value of the quadratic term in the gain expression gives a too broad Hermite-Gauss solution and results in high values of the perturbation terms. This gives "ears" on the intensity distribution which reduce the differential efficiency.

The theory presented in [6] is based on the parabolic approximation. The permittivity is assumed to be a combination of a constant part and a current dependent part. In case of an offset between these two parts the theory predicts both kinks and near-field shifts, as observed experimentally. Furthermore, the theory has the advantage that the calculations can be carried out without a large computer.

In the present paper we have taken advantage of the (ideal) symmetry of the laser structure in order to simplify the calculations; consequently, all calculated near fields are symmetrical. The near fields are always found to be stable and the kinks are associated with higher order modes. Very good agreement with the results for the (slightly asymmetrical) "well behaved" laser reported in [6] is obtained.

The type of kink described in [6] only involves the fundamental mode. For relatively narrow lasers ($2S \lesssim 15$ μm), this may be the dominating mechanism, since the kinks tend to appear at lower power levels than the kinks calculated by the present model.

VI. CONCLUSION

The present model describes the static behavior of DH lasers in detail. Very few assumptions have been necessary and precise methods are used. By this model it is possible to predict the properties of lasers directly from the technological parameters when the material parameters are known. It will also be possible to optimize the lasers with respect to threshold current, efficiency, linearity, etc.

It is shown that kinks may appear in ideal lasers.

APPENDIX
NUMERICAL SOLUTION OF THE DIFFUSION EQUATION

From (17) we see that $A'(y)$ is constant and $B'(y)$ is zero for large y values. For an ideal symmetrical laser the boundary conditions are

$$\frac{dN}{dy}\bigg|_{y=0} = 0, \qquad N(y) \longrightarrow 0 \text{ for } y \longrightarrow \infty. \qquad (A1)$$

We consider discrete points

$$y_i, i = 0, 1, \cdots, M$$

$$y_0 = 0, \qquad \Delta y = y_{i+1} - y_i$$

$$A'(y) = A'(y_M), \qquad B'(y) = 0 \qquad \text{for } y \geqslant y_M. \qquad (A2)$$

We expand the second derivative and use the boundary conditions

$$\frac{d^2N}{dy^2} = \frac{1}{(\Delta y)^2}(N(y_{i+1}) - 2N(y_i) + N(y_{i-1})) \qquad (A3)$$

$$\frac{d^2N}{dy^2}\bigg|_{y=0} = \frac{2}{(\Delta y)^2}(N(y_1) - N(y_0)) \qquad (A4)$$

$$N(y_{M+1}) = N(y_M) e^{-\sqrt{A'(y_M)}\,\Delta y} \qquad (A5)$$

Equation (17) is transformed into a set of $M+1$ linear equations with the $M+1$ unknowns $N(y_0), N(y_1), \cdots, N(y_M)$. This set of equations can be written

$$\overline{\overline{C}} \cdot \overline{N} = \overline{B}$$

$$\overline{N} = (N(y_0), N(y_1), \cdots, N(y_M))$$

$$\overline{B} = (\Delta y)^2 (\tfrac{1}{2} B'(y_0), B'(y_1), \cdots, B'(y_{M-1}), 0)$$

$$= (d_0, d_1, \cdots, d_M) \qquad (A6)$$

$$C_{rs} = \begin{cases} 1 + \dfrac{A'(y_0)}{2}(\Delta y)^2 & r = s = 0 \\[2mm] 2 + A'(y_r)(\Delta y)^2 & r = s, s = 1, \cdots, M-1 \\[2mm] 2 + A'(y_M)(\Delta y)^2 - e^{-\sqrt{A'(y_M)}\,\Delta y} & \\ & r = s = M \\[2mm] -1 & \begin{cases} r = s - 1, s = 1, \cdots, M \\ r = s + 1, s = 0, \cdots, M-1 \end{cases} \\[4mm] 0 & \text{elsewhere.} \end{cases}$$

Since $\overline{\overline{C}}$ is a tridiagonal matrix, $\overline{N}$ is easily found using the following procedure:

$$\overline{C} = (c_0, c_1, \cdots, c_M) = (C_{00}, C_{11}, \cdots, C_{MM})$$

$$\overline{C}' = (c_0', c_1', \cdots, c_M')$$

$$\overline{D}' = (d_0', d_1', \cdots, d_M')$$

$$\left. \begin{array}{ll} c_0' = \dfrac{1}{c_0} & c_i' = \dfrac{1}{c_i - c_{i-1}'} \\[2mm] d_0' = d_0 c_0' & d_i' = (d_i + d_{i-1}')c_i' \end{array} \right\} \quad i = 1, \cdots, M$$

$$N(y_M) = d_M'$$

$$N(y_i) = d_i' + c_i' N(y_{i+1}) \qquad i = M-1, \cdots, 0.$$

By this method precise results are obtained very quickly.

REFERENCES

[1] G. B. Hocker and W. K. Burns, "Mode dispersion in diffused channel waveguides by the effective index method," *Appl. Opt.*, vol. 16, pp. 113–118, 1977.
[2] J. Buus, "Detailed field model for DH stripe lasers," *Opt. Quant. Elec.*, vol. 10, Nov. 1978.
[3] W. O. Schlosser, "Gain induced modes in planar structures," *Bell Syst. Tech. J.*, vol. 52, pp. 887–905, 1973.
[4] T. L. Paoli, "Waveguiding in a stripe-geometry junction laser," *IEEE J. Quantum Electron.*, vol. QE-13, pp. 662–668, 1977.
[5] A. G. Steventon, P. J. Fiddyment, and D. H. Newman, "Low threshold current proton-isolated (GaAl)As double heterostructure lasers," *Opt. Quant. Elec.*, vol. 9, pp. 519–525, 1977.
[6] G. H. B. Thompson, D. F. Lovelace, and S. E. M. Turley, "Kinks' in the light/current characteristics and near field shifts in (GaAl)As heterostructure stripe lasers and their explanation by the effect of self-focusing on a built-in optical waveguide," *Inst. Elec. Eng. Solid-State Elect. Dev.*, vol. 2, pp. 12–30, 1978.
[7] N. Chinone, "Nonlinearity in power-output-current characteristics of stripe-geometry injection lasers," *J. Appl. Phys.*, vol. 48, pp. 3237–3244, 1977.
[8] W. Streifer, D. R. Scifres, and R. D. Burnham, "Analysis of gain-induced waveguiding in stripe geometry diode lasers," *IEEE J. Quantum Electron.*, vol. QE-14, pp. 418–427, 1978.
[9] W. P. Dumke, "Current thresholds in stripe-contact injection lasers," *Solid-State Electron.*, vol. 16, pp. 1279–1284, 1973, also in W. B. Joyce and S. H. Wemple, "Steady-state junction-current distributions in thin resistive films on semiconductor junction (solutions of $\nabla^2 v = \pm e^v$)," *J. Appl. Phys.*, vol. 41, pp. 3818–3830, 1970.
[10] W. B. Joyce and R. W. Dixon, "Thermal resistance of heterostructure lasers," *J. Appl. Phys.*, vol. 46, pp. 855–862, 1975.